Journal of Catalysis 257 (2008) 5–15

Contents lists available at ScienceDirect

Journal of Catalysis

www.elsevier.com/locate/jcat

Synthesis and characterization of Pt clusters in aqueous solutions

Attilio Siani, Karen R. Wigal, Oleg S. Alexeev *, Michael D. Amiridis *

Department of Chemical Engineering, University of South Carolina, Columbia, SC 29208, USA

ARTICLE INFO

Article history:
Received 21 January 2008
Revised 27 March 2008
Accepted 27 March 2008
Available online 21 May 2008

Keywords:
Colloidal platinum
Pt clusters
PVA
EXAFS
Propanol oxidation

ABSTRACT

Extended X-ray absorption fine structure (EXAFS) and UV–visible (UV–vis) spectroscopies were used to monitor the various steps involved in the synthesis of unprotected and poly(vinyl alcohol) (PVA)-protected aqueous colloidal Pt suspensions. The results indicate that on hydrolysis of the H_2PtCl_6 precursor, the Cl^- ligands were partially replaced by aquo ligands in the first coordination shell of Pt to form $[PtCl_2(H_2O)_4]^{2+}$. Treatment of these species with $NaBH_4$ under controlled pH conditions led to the formation of nearly uniform Pt_4 and Pt_6 clusters in the absence and presence of PVA, respectively. These highly dispersed colloidal Pt suspensions were stable for several months. The addition of 2-propanol (IPA) to both types of Pt suspensions led to some sintering of the Pt clusters, although both suspensions retained their colloidal nature. Less sintering was evident in the PVA-protected Pt suspension. Both the unprotected and the PVA-protected colloidal Pt suspensions were catalytically active for the liquid-phase selective oxidation of 2-propanol to acetone, with the unprotected suspension exhibiting the highest activity.

1. Introduction

Colloidal suspensions of different metals have found applications in various fields, including nanoelectronics and optics [1]. Such colloidal suspensions also are used in the field of catalysis, because a large fraction of the catalytically active metal sites in this case is exposed to the reactants. Interest in these materials is significant because they are used in reactions of industrial relevance, such as the selective hydrogenation and oxidation of various organic compounds [1].

Conventional methods used for the preparation of colloidal metal suspensions require the chemical reduction of transition metal salts in an aqueous or organic medium, typically performed in the presence of surfactants, which act as protective agents [1–3]. The use of protective agents is necessary to preserve the colloidal nature of the solution, because the metal nanoparticles formed are usually unstable and tend to form larger aggregates, which can precipitate from the solution. Several chemical compounds, including poly(vinyl pyrrolidone) (PVP), poly(vinyl alcohol) (PVA), polyoxoanions, and other organic molecules containing phosphine or amine groups, have been used in this role [1–3]. However, it has been reported that such protective agents can act as poisons by strongly interacting with the metal nanoparticles, thereby reducing their catalytic efficiency [4].

The goal of the present work was to develop a novel synthetic approach for the preparation of nearly uniform Pt clusters in aqueous solutions without the use of any surfactants or protective agents. The advantage of such an approach is that it eliminates the potential poisoning of active metal sites by the protective agents. UV–vis and EXAFS spectroscopies were used to characterize the local coordination environment of Pt in the colloidal solutions. Finally, the catalytic activity of the colloidal Pt was evaluated for the liquid-phase selective oxidation of 2-propanol to acetone.

2. Experimental

2.1. Reagents and materials

$H_2PtCl_6 \cdot 6H_2O$ (99.95% purity, Alfa Aesar), sodium borohydride (98% purity, Alfa Aesar), 2-propanol (99.8% purity, Sigma-Aldrich), and low molecular weight PVA (Alfa Aesar) were used as supplied. 18 MΩ cm Milli-Q deionized water was used for the preparation of all aqueous solutions.

2.2. Preparation of unprotected colloidal Pt suspensions

Appropriate amounts of $H_2PtCl_6 \cdot 6H_2O$ were dissolved in deionized water to obtain solutions with a platinum concentration of $2.6 \cdot 10^{-4}$ M. The resulting solutions, characterized by a yellow color and a pH of approximately 3.3 after aging, were subsequently reduced under vigorous stirring with freshly prepared aqueous solutions of sodium borohydride ($NaBH_4$). The $NaBH_4$/Pt weight ratio was fixed to 3. After the reduction step was completed, the aque-

* Corresponding authors.
E-mail addresses: alexeev@engr.sc.edu (O.S. Alexeev), amiridis@engr.sc.edu (M.D. Amiridis).

0021-9517/$ – see front matter
doi:10.1016/j.jcat.2008.03.024

ous solutions had a brown color and were characterized by a neutral pH. The resulting platinum colloids were found to be stable with no signs of Pt precipitation or color change over a period of more than 24 months.

2.3. Preparation of PVA-protected colloidal Pt suspensions

Appropriate amounts of PVA were dissolved in deionized water to obtain solutions containing 10 mg/ml of PVA. These solutions were subsequently mixed with aqueous solutions of $H_2PtCl_6 \cdot 6H_2O$ containing $2.6 \cdot 10^{-4}$ M of platinum, yielding final solutions with a PVA/Pt weight ratio of 1. A similar procedure was also used to prepare solutions with a PVA/Pt weight ratio of 2. Both types of solutions were further treated with freshly prepared solutions of $NaBH_4$ ($NaBH_4$/Pt weight ratio of 3) under vigorous stirring. The colloidal platinum suspensions thus obtained had a brown color, a neutral pH, and were stable with no signs of Pt precipitation or color change over a period of more than 24 months.

2.4. UV–vis spectroscopy

UV–vis spectra were obtained using a Shimadzu UV-2101PC spectrophotometer. The scan range was 800–190 nm in steps of 0.5 nm. Unless stated otherwise, 18 MΩ cm water (Milli-Q grade) was used as the reference for all measurements.

2.5. 2-Propanol oxidation

The oxidation of 2-propanol (IPA) in air was conducted in a batch reactor at 14 °C under atmospheric pressure. The concentration of Pt in the reactor was $2.6 \cdot 10^{-4}$ M, and the initial concentration of IPA was varied in the range of 0.05–0.2 M. The appearance of acetone in the solution was characterized by UV–vis spectroscopy, monitoring the intensity of the acetone band at 265 nm.

2.6. EXAFS spectroscopy

EXAFS spectra were collected at X-ray beamline 2–3 at the Stanford Synchrotron Radiation Laboratory (SSRL), Stanford Linear Accelerator Center, Menlo Park, CA. The storage ring electron energy was 3 GeV, and the ring current was in the range of 80–100 mA. The EXAFS data for aqueous solutions were recorded at room temperature in the fluorescence mode with a 13th-element Ge detector. Liquid samples were loaded into *in situ* EXAFS cells designed to allow handling of samples without air exposure. The total count rate for the Ge detector was in the range of 30,000–40,000 counts/s. It has been established experimentally that the detector readings are linear within this range and that no corrections for dead-time are required. Samples were scanned at the Pt L_3 edge (11564 eV). Data were collected with a Si(220) double-crystal monochromator, which was detuned by 30% to minimize the effects of higher harmonics in the X-ray beam.

2.7. EXAFS data analysis

The EXAFS data were analyzed with experimentally determined reference files obtained from EXAFS data characterizing materials of known structure. More specifically, the Pt–Pt, Pt–Cl, and Pt–O interactions were analyzed with phase shifts and backscattering amplitudes obtained from EXAFS data characterizing platinum foil, K_2PtCl_4, and $Na_2Pt(OH)_6$, respectively. The crystallographic first-shell coordination parameters for these reference compounds, the weighting of the Fourier transform, and the ranges in k and r space used to extract the reference functions from the experimental EXAFS data are reported in Table 1. The EXAFS parameters were extracted from the raw data with the aid of the XDAP software [5]. The methods used to extract the EXAFS function from the raw data are essentially the same as those reported elsewhere [6]. The data used for each sample were the averages of six scans.

Table 1
Crystallographic data and Fourier filtering ranges used for reference compounds

Sample	Crystallographic data			Fourier transform		
	Shell	N	R (Å)	Δk (Å^{-1})	Δr (Å)	n
Pt foil	Pt–Pt first	12	2.77	1.9–16.5	1.9–3.0	3
$Na_2Pt(OH)_6$	Pt–O	6	2.05	1.4–16.5	0.5–2.0	3
K_2PtCl_4	Pt–Cl	4	2.31	1.9–15.9	1.0–2.7	3

Note. N, coordination number for absorber–backscatterer pair; R, distance; Δk, limits used for forward Fourier transform (k is the wave vector); Δr, limits used for the shell isolation (r is the distance); n, power of k used for Fourier transformation.

The data at the Pt L_3 edge were analyzed with a maximum of 16 free parameters over the ranges $3.50 < k < 15.00$ Å^{-1} (where k is the wave vector) and $1.00 < r < 3.50$ Å (where r is the distance from the absorbing Pt atom). The statistically justified number of free parameters, n, was found to be 19, as estimated on the basis of the Nyquist theorem [7,8]: $n = (2\Delta k \Delta r/\pi) + 1$, where Δk and Δr are the k and r ranges used to fit the data. The parameters characterizing both the high-Z (Pt–Pt) and low-Z (Pt–O) contributions for the samples examined were determined by multiple-shell fitting in r-space with application of k^1 and k^3 weighting in the Fourier transformations [6]. The fit was optimized using a difference file technique with phase- and amplitude-corrected Fourier transformations of the data [9,10]. Comparisons of the data and fits for key samples in r-space are shown in Figs. 1 and 2, and the results are summarized in various tables presented later in the paper. Standard deviations reported in these tables for the various parameters were calculated from the covariance matrix, taking into account the statistical noise of the EXAFS data, as well as the correlations among the different coordination parameters, as described elsewhere [11]. Systematic errors were not included in the calculation of the standard deviations. The values of the goodness of fit (ε_v^2) were calculated as outlined in the Reports on Standards and Criteria in XAFS Spectroscopy [12]. The variances in both the imaginary and absolute parts were used to evaluate the quality of the fit [13].

2.8. XANES measurements and analysis

X-ray absorption near-edge (XANES) spectra of each sample were also obtained during the X-ray absorption measurements described above. Normalized XANES spectra were obtained by subtracting the pre-edge background from the raw data using a modified Victoreen equation, and dividing the absorption intensity by the height of the absorption edge. The band structure curves were numerically integrated using the XDAP software [5]. The observed band structure for the Pt L_3 edge, commonly called the "white line," indicates absorption threshold resonances associated with the likelihood of excitations of $2p_{3/2}$ electrons to unoccupied d states [14]. It is generally assumed that the white line correlates with the electron density of metal atoms, with a decrease in the white line area indicating a decrease in the electron density of these atoms [14,15].

3. Results and discussion

3.1. Synthesis of unprotected Pt colloids

The interaction of H_2PtCl_6 with H_2O leads to a series of hydrolysis reactions, during which the octahedral coordination of Pt(IV) remains intact [16–18]. In this process, some Cl^- ligands from the coordination shell of Pt are replaced by water molecules. This step

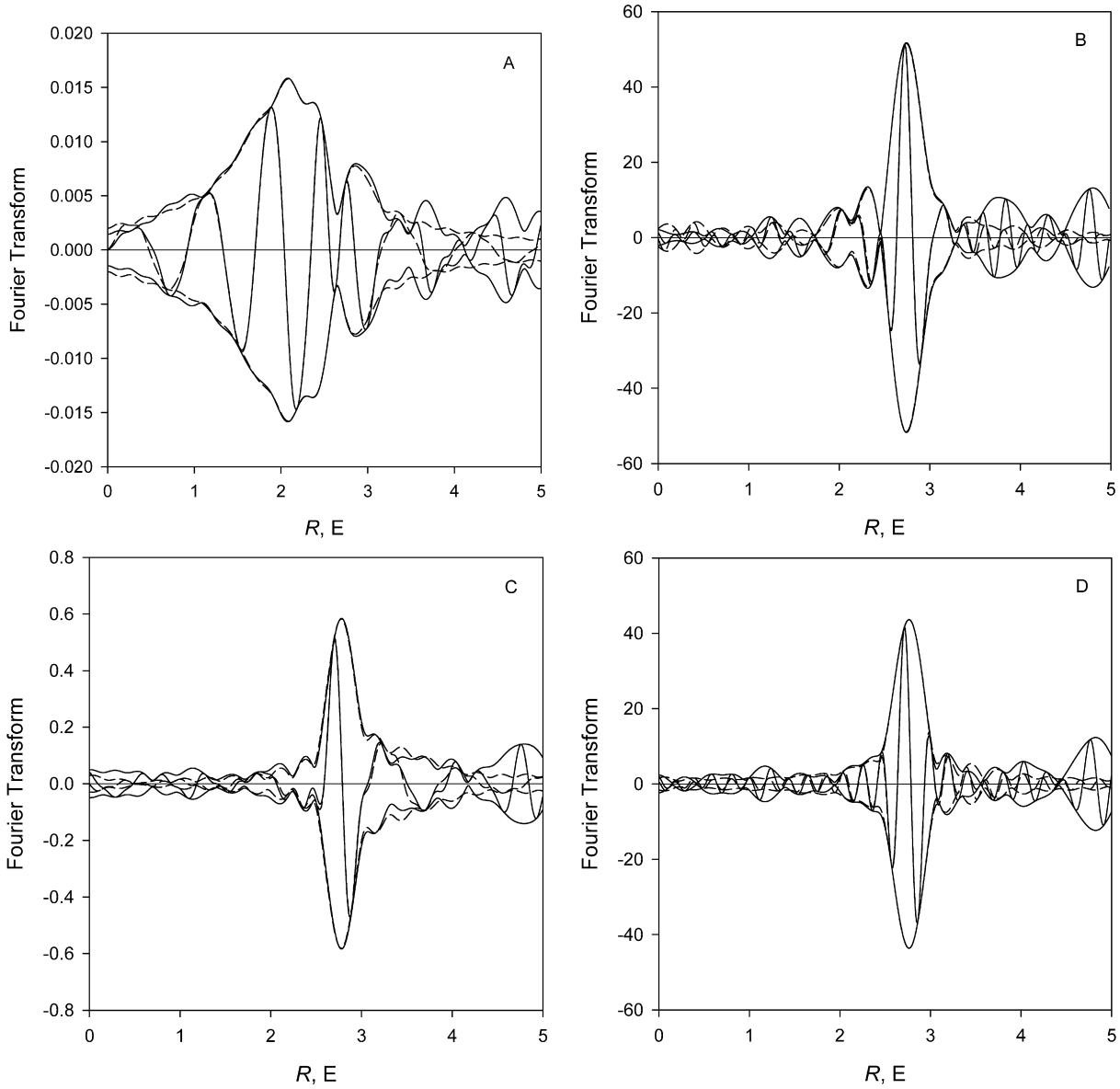

Fig. 1. EXAFS spectrum collected at the Pt L_3 edge and corresponding fits for an unprotected colloidal Pt suspension formed following the treatment of a $2.6 \cdot 10^{-4}$ M H_2PtCl_6 aqueous solution with $NaBH_4$ at room temperature: (A) imaginary part and magnitude of uncorrected Fourier transform (k^0-weighted, $\Delta k = 3.5$–15.0 Å^{-1}) of experimental EXAFS (solid line) and sum of the calculated contributions as stated in Table 2 (dashed line); (B) k^3-weighted Fourier transform of (A) plotted with Pt–Pt phase and amplitude correction; (C) and (D) residual spectra illustrating the Pt–Pt contributions: the imaginary part and magnitude of phase- and amplitude-corrected Fourier transforms (k^1 weighted (C) and k^3 weighted (D)) of the raw data minus Pt–O contributions (solid line) and the calculated first-shell Pt–Pt contributions (dashed line).

is followed by a slow H_2O–OH^- exchange, leading to the formation of $[PtCl_{6-x}(OH)_y^-(H_2O)_{x-y}]^{-2+x-y}$ species. The degree of hydrolysis strongly depends on the solution pH, the concentration of H_2PtCl_6, and the presence of other anions [16]. We previously used EXAFS to characterize an aqueous solution containing $1.2 \cdot 10^{-3}$ M of H_2PtCl_6 [19,20]. The results indicated that the first coordination shell of Pt consists, on average, of three chlorine atoms at a Pt–Cl distance of 2.31 Å and three oxygen atoms at a Pt–O distance of 2.01 Å, suggesting the formation of $[PtCl_3(H_2O)_3]^+$ species.

When a substantially lower concentration of H_2PtCl_6 is used, a higher degree of hydrolysis is expected [12,18]. Indeed, the EXAFS data summarized in Table 2 for an aqueous solution of H_2PtCl_6 with a Pt concentration of $2.6 \cdot 10^{-4}$ M indicate the presence of approximately 1.5 chlorine atoms and 4.3 oxygen atoms in the first coordination shell of Pt at average Pt–Cl and Pt–O_1 distances of 2.33 and 2.05 Å, respectively. Overall, the EXAFS data suggest that the hydrolysis of H_2PtCl_6 on average led to the formation of $[PtCl_2(H_2O)_4]^{2+}$ species, in which the Pt^{4+} cations retain their octahedral coordination, consistent with previous literature reports [16–20]. In addition to the first-shell Pt–O_1 contributions, Pt–O_2 contributions with an average coordination number of 7.5 at an average distance of approximately 2.99 Å were also observed in the EXAFS spectra (Table 2). These contributions represent interactions between water molecules of the second solvation shell with the $[PtCl_2(H_2O)_4]^{2+}$ units [19–21].

The UV–vis absorption spectrum characterizing the solution containing $[PtCl_2(H_2O)_4]^{2+}$ species (Fig. 3, spectrum 1) consisted of two strong bands at 210 and 260 nm, which can be assigned to the Pt^{4+}–O and Pt^{4+}–Cl ligand-to-metal charge transfer, respectively [22]. When this solution was further treated with $NaBH_4$, its color changed from yellow to dark brown and the UV–vis spectrum showed the presence of a single band at 215 nm (Fig. 3, spectrum 2). The position of this band is consistent with the results of calculations performed based on Mie's theory for the in-

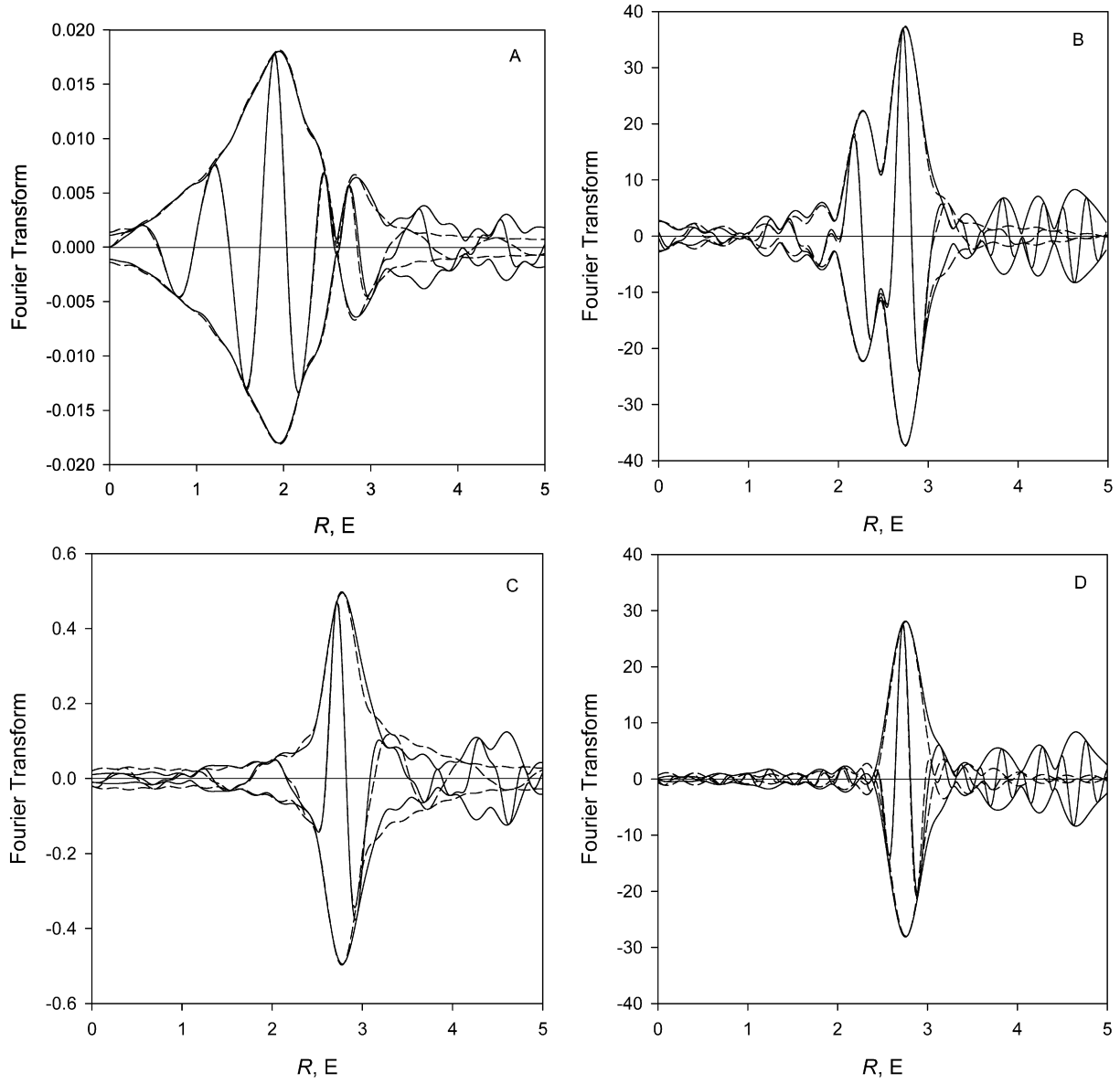

Fig. 2. EXAFS spectrum collected at the Pt L_3 edge and corresponding fits for a PVA-protected colloidal Pt suspension formed following the treatment of a $2.6 \cdot 10^{-4}$ M H_2PtCl_6 aqueous solution in the presence of PVA with $NaBH_4$ at room temperature: (A) imaginary part and magnitude of uncorrected Fourier transform (k^0-weighted, $\Delta k = 3.5$–15.0 Å^{-1}) of experimental EXAFS (solid line) and sum of the calculated contributions as stated in Table 2 (dashed line); (B) k^3-weighted Fourier transform of (A) plotted with Pt–Pt phase and amplitude correction; (C) and (D) residual spectra illustrating the Pt–Pt contributions: the imaginary part and magnitude of phase- and amplitude-corrected Fourier transforms (k^1 weighted (C) and k^3 weighted (D)) of the raw data minus Pt–O contributions (solid line) and the calculated first-shell Pt–Pt contributions (dashed line).

teractions of the conduction band electrons of Pt particles with an electromagnetic radiation [2]. A similar absorption band was previously observed in the UV–vis spectra of Pt colloids prepared through radiolysis and hydrogen reduction treatments of aqueous solutions of K_2PtCl_4 in the presence of stabilizing agents and was associated with the presence of isolated Pt clusters [23]. Indeed, reduction of Pt^{4+} to Pt^0 is expected on treatment of an aqueous solution containing $[PtCl_2(H_2O)_4]^{2+}$ species with $NaBH_4$ [1]. Based on the above, we propose that the absorption band observed in the UV–vis spectrum at 215 nm is associated with the formation of reduced Pt particles or clusters.

The EXAFS data summarized in Table 2 for the aqueous solution of H_2PtCl_6 treated with $NaBH_4$ are consistent with the UV–vis results discussed in the previous paragraph. The EXAFS results show that the $NaBH_4$ treatment removed all chlorine atoms from the first coordination shell of Pt, as indicated by the lack of Pt–Cl contribution in the EXAFS spectra. Instead, approximately 3.1 platinum atoms at an average Pt–Pt distance of 2.72 Å were observed in the first coordination shell of Pt. Because no higher Pt–Pt shells were detected, these results suggest the formation of nearly uniform Pt clusters that are largely isolated from one another and incorporate approximately four metal atoms. The presence of Pt–O_1 and Pt–O_2 contributions at average distances of 2.06 and 2.84 Å, respectively, is indicative of interactions of these small Pt clusters with the aquo species in the solution. Furthermore, the analysis of the XANES region of the spectra provides valuable information regarding the electronic structure of Pt, as described previously [14,15]. Fig. 4 provides a direct comparison of the XANES regions for the unprotected colloidal Pt solution, a Pt foil, and Pt^{2+} cations. Integration of the white line areas, summarized in Table 3, indicate that the relatively high white line area observed for the H_2PtCl_6 solution containing Pt^{4+} cations decreased from 11 to approximately 4 af-

Table 2
Structural parameters characterizing various Pt-containing aqueous solutions

Sample	Shell	N	R (Å)	$\Delta\sigma^2$ (Å^2)	ΔE_0 (eV)	ε_v^2	k^1-variances (%)		Suggested model for the species formed
							Abs	Im	
H_2PtCl_6/H_2O	Pt–Pt	–	–	–	–	3.7	1.6	3.7	Pt^{4+} cations in octahedral environment
	Pt–Cl	1.5	2.33	0.00139	−9.9				
	Pt–O_1	4.3	2.05	0.00310	2.7				
	Pt–O_2	7.5	2.99	0.01000	7.5				
H_2PtCl_6/H_2O treated with $NaBH_4$ at 25 °C	Pt–Pt	3.1	2.72	0.00325	−6.9	3.0	2.4	3.9	Pt_4 clusters
	Pt–Cl	–	–	–	–				
	Pt–O_1	1.9	2.02	0.01000	6.9				
	Pt–O_2	7.3	2.84	0.01000	−10.0				
H_2PtCl_6/H_2O treated with $NaBH_4$ at 25 °C in the presence of PVA	Pt–Pt	4.1	2.73	0.00581	−6.1	4.6	1.2	2.0	Pt_6 clusters
	Pt–Cl	–	–	–	–				
	Pt–O_1	0.4	2.01	−0.00160	0.15				
	Pt–O_2	6.0	2.25	0.00659	−8.9				
	Pt–O_3	8.7	2.45	0.00895	7.0				

Note. N, coordination number; R, distance between absorber and backscatterer atoms; $\Delta\sigma^2$, difference in Debye–Waller factors between the sample and the reference compound; ΔE_0, inner potential correction accounting for the difference in the inner potential between the sample and the reference compound; ε_v^2, goodness of fit. Standard deviations in fits: $N \pm 20\%$, $R \pm 1\%$, $\Delta\sigma^2 \pm 5\%$, $\Delta E_0 \pm 10\%$.

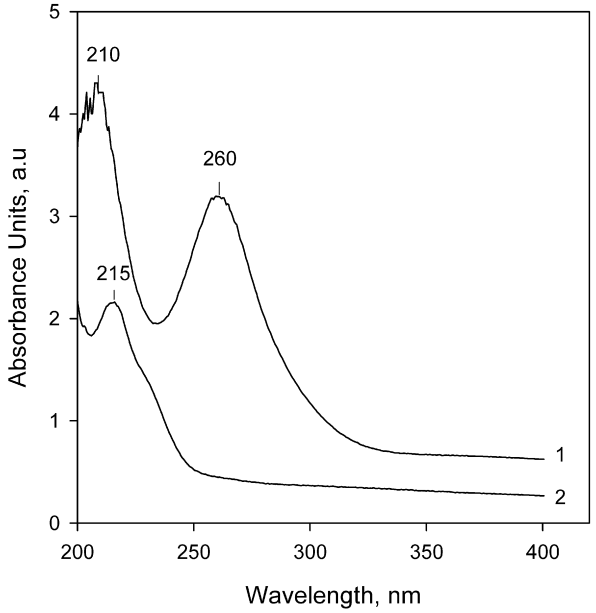

Fig. 3. UV–vis absorption spectra of aqueous solutions of: (1) H_2PtCl_6 ($2.6 \cdot 10^{-4}$ M), (2) unprotected colloidal Pt suspension ($2.6 \cdot 10^{-4}$ M).

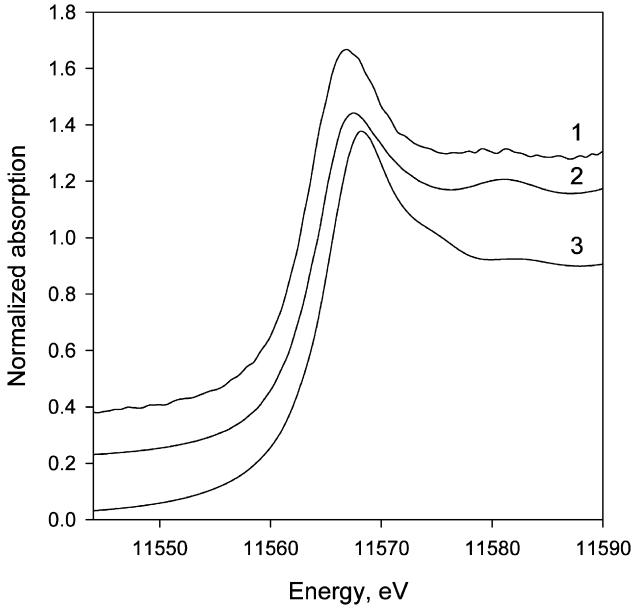

Fig. 4. Pt L_3 absorption edge of (1) unprotected colloidal Pt solution, (2) Pt foil, and (3) $[Pt(NH_3)_4]Cl_2$.

ter the treatment with $NaBH_4$. This value is substantially smaller than a corresponding value of 7 observed for the K_2PtCl_4 solution containing Pt^{2+} cations and is very close to the value obtained with Pt foil (i.e., 3.8), suggesting that the Pt clusters formed in the solution are in a metallic state.

Previous literature reports indicate that attempts to form Pt colloids without the use of stabilizing agents usually lead to the precipitation of Pt from the solution. Nearly featureless UV–vis spectra with a weak maximum at 260 nm were obtained in this case [23]. In contrast, our unprotected colloidal solution with a Pt concentration of approximately $2.6 \cdot 10^{-4}$ M was characterized by an absorption band at 215 nm and remained unchanged for approximately 24 months with no Pt precipitate detected, despite exposure to light and air. This surprising result can be attributed to both the low concentration of H_2PtCl_6 in the solution and to the use of $NaBH_4$ as the reducing agent. In fact, when the concentration of H_2PtCl_6 in this unprotected solution was doubled (i.e., to $5 \cdot 10^{-4}$ M), a Pt precipitate was formed after the treatment with $NaBH_4$. In addition, when H_2 was used as the reducing agent, a Pt precipitate was formed even when the concentration of H_2PtCl_6 was maintained at $1.3 \cdot 10^{-4}$ M.

Table 3
XANES data for various Pt samples in solution and on a γ-Al_2O_3 support

Experiment	Sample	White line area (eV)	Reference
S0	Pt foil	3.8	[17]
S1	H_2PtCl_6/H_2O	11.2	This work
S2	K_2PtCl_4/H_2O	7.0	[17]
S3	S1 treated with $NaBH_4$ at 25 °C	4.3	This work
S4	S1 treated with $NaBH_4$ at 25 °C in the presence of PVA	4.6	This work
S5	S3 exposed to 2-propanol/O_2 for 4 h	4.3[a]	This work
S6	S4 exposed to 2-propanol/O_2 for 4 h	4.2[a]	This work

[a] Average values of the white line area under reaction conditions.

It is possible that the absence of Pt precipitation from the $2.6 \cdot 10^{-4}$ M solution treated with $NaBH_4$ can be attributed to the very low ionic strength of the solution (approximately $4.8 \cdot 10^{-3}$ M)

under our experimental conditions, consistent with literature reports indicating that the precipitation of Pt from Pt colloids begins when the value of ionic strength exceeds 10^{-2} M [24,25]. In general, an increase in ionic strength leads to a lowering of the coagulation barrier and consequently to metal precipitation [1]. Another possible explanation is related to the electrostatic stabilization of the Pt clusters, arising from their interactions with ionic compounds present in the solution. As reported previously, aggregation and precipitation of metal colloids occurs due to van der Waals forces, which attract metal particles to one another in solution [1–3]. The adsorption of ionic compounds and their related counterions on the surface of metal particles generates an electrical double layer around the particles, resulting in Coulombic repulsions [1]. With a sufficiently high electric potential in such a double layer, the electrostatic repulsion counterbalances the van der Waals forces, possibly preventing the aggregation of metal particles [1]. The nature and origin of the ions responsible for this double layer are not immediately apparent; we explored several possibilities.

The formation of metal clusters from isolated zero-valent metal atoms is not thermodynamically favored in solutions [26,27] and can be ruled out as a growth mechanism for Pt and other noble metals. Instead, it has been suggested that for these metals, the formation of clusters in solutions occurs through a surface-growth mechanism in which metal ions are adsorbed on the cluster surface and reduced *in situ* [26]. Therefore, in our case, the formation of Pt clusters can be rationalized by the stepwise reduction of $PtCl_6^{2-}$ to $PtCl_4^{2-}$ and Pt^0 atoms on the surface of some Pt nucleation sites formed during the initial stages of the reduction [26,28]. Any chlorine ligands not released during this process also could provide some electrostatic repulsion and thus be responsible, at least in part, for the electrostatic stabilization of the Pt clusters formed. But our EXAFS data characterizing the H_2PtCl_6 solution treated with $NaBH_4$ clearly indicate the absence of any chlorine ligands in the first coordination shell of Pt (Table 2). Moreover, theoretical calculations suggest that the presence of water and chlorine ligands is not sufficient to stabilize noble metal cores into a stable geometry in solution [26]. Therefore, in our case, we need to explore other options for the electrostatic stabilization of Pt clusters.

Literature reports indicate that the stability of Pt colloids prepared by the citrate reduction of H_2PtCl_6 is influenced significantly by the nature of cations present in the solution (e.g., Na^+, Mg^{2+}, Al^{3+}), whereas the effect of the valence and the nature of anions present (e.g., Cl^-, carbonate, sulfate) is relatively small [24,25]. Among monovalent, divalent, and trivalent cations, the monovalent ones were found to improve the stability of Pt colloids significantly [24]. Moreover, among different combinations of various cations and anions, relatively high concentrations of NaCl (i.e., $>1.2 \cdot 10^{-2}$ M) were required to destabilize the Pt colloid and induce Pt precipitation [24,25]. Both Na^+ and Cl^- species were present in the solution during our experiments; therefore, it is likely that the combination of these species could be responsible for the electrostatic stabilization of the Pt clusters formed. Moreover, the maximum concentration of these species did not exceed $7.9 \cdot 10^{-3}$ M under our experimental conditions, which is below the limit required to destabilize the Pt colloid [24,25]. Finally, we should not ignore the presence of borate species in the solution under our experimental conditions. To the best of our knowledge, the effect of these species on the stability of metal colloids has not been evaluated previously. Our data lead us to conclude that concentrations of these species at up to $7.9 \cdot 10^{-3}$ M are not affecting the stability of the Pt colloids formed in any negative way; whether their presence has a stabilizing effect remains an open question.

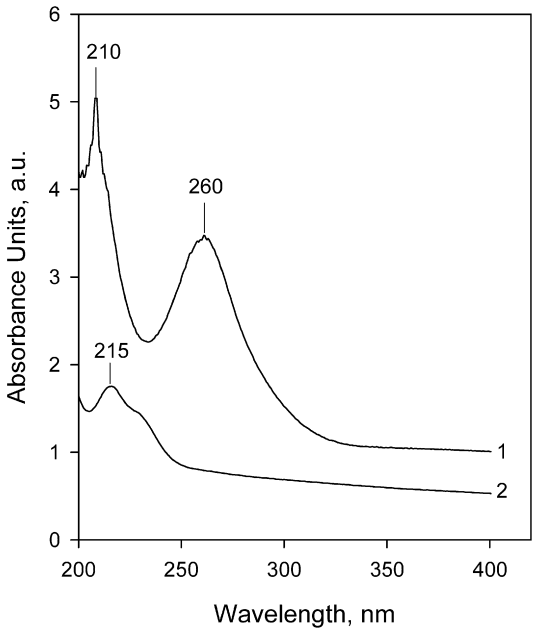

Fig. 5. UV–vis absorption spectra of aqueous solutions of: (1) H_2PtCl_6 ($2.6 \cdot 10^{-4}$ M) in the presence of PVA (10 mg/ml), (2) following treatment with $NaBH_4$ at room temperature.

3.2. Synthesis of Pt colloids stabilized by PVA

The various steps involved in the preparation of Pt colloids stabilized by PVA were also characterized by UV–vis and EXAFS spectroscopy. When a 10-mg/ml solution of PVA was added to an aqueous solution containing $2.6 \cdot 10^{-4}$ M of H_2PtCl_6 and the solution was further treated with $NaBH_4$, the color of the solution changed from yellow to dark brown, and the UV–vis spectrum consisted of a single peak at 215 nm (Fig. 5). Similar to the case of the Pt colloidal solution prepared in the absence of PVA, the presence of this peak may indicate the formation of isolated Pt clusters, in agreement with previous reports [23].

The EXAFS data collected for this sample at the Pt L_3 edge (Table 2) support such a conclusion. More specifically, the presence of only first-shell Pt–Pt contributions with an average coordination number of 4.1 at a bond distance of 2.73 Å is consistent with the formation of isolated and nearly uniform Pt clusters incorporating on average approximately 6 metal atoms. These results also suggest that slightly larger Pt clusters were formed in the presence of PVA, and thus, PVA may promote the nucleation of Pt atoms to some degree. Multiple Pt–O contributions observed in the spectra with average coordination numbers of 0.4, 6.0, and 8.7 at bonding distances of 2.01, 2.25, and 2.45 Å, respectively, may indicate the presence of aquo ligands around Pt; however, some of these contributions also can be attributed to interactions between Pt atoms and hydroxyl groups of the PVA macromolecules, creating a protective layer around the Pt clusters [1]. At this point, it is not possible to distinguish these contributions from those of aquo ligands.

Similar to the case of the unprotected colloidal Pt solution, the analysis of the XANES region yields a value of 4.6 for the white line area (Table 3), which is substantially smaller than the corresponding values for Pt^{4+} and Pt^{2+} cations in aqueous solutions and close to that of Pt foil. Once again, this result suggests the formation of reduced Pt species.

3.3. Aggregation of Pt clusters in solution

The stability of highly dispersed Pt colloids was subsequently evaluated in the presence of IPA, in preparation for conducting cat-

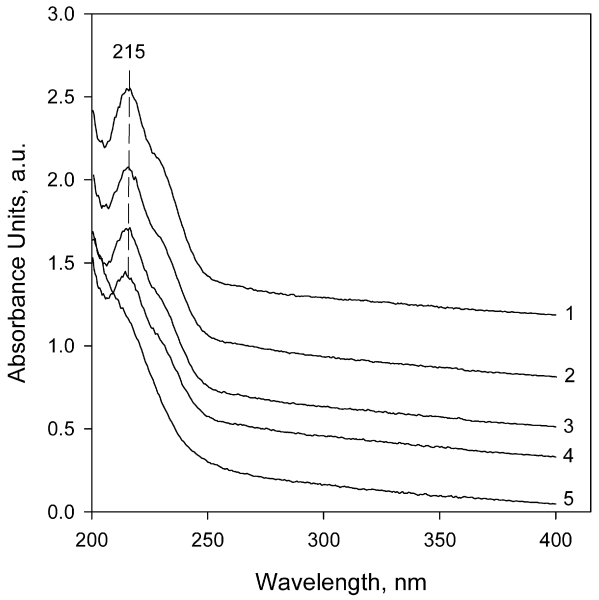

Fig. 6. UV–vis absorption spectra of an unprotected colloidal Pt suspension collected at: (1) 0, (2) 5, (3) 10, (4) 20, and (5) 30 min after the addition of IPA.

alytic experiments of the oxidation of IPA. When 0.2 M of IPA was added at room temperature to a freshly prepared unprotected colloidal Pt suspension containing Pt_4 clusters, the dark-brown color of the solution became more intense. This change was accompanied by a gradual decrease in the intensity of the 215-nm band in the UV–vis spectra over a period of 30 min (Fig. 6). After this period, the 215-nm band nearly disappeared from the spectrum, which remained unchanged thereafter, indicating that the solution was stabilized.

EXAFS results obtained with this sample are summarized in Table 4 and indicate that substantial aggregation of the Pt_4 clusters occurred after the addition of IPA to the solution. More specifically, the first-shell Pt–Pt coordination number increased from approximately 3.1 to 7.4 on introduction of IPA, indicating the formation of Pt nanoparticles with an average diameter of approximately 1.4 nm [29].

IPA can have two main effects on the dispersion of Pt in the colloidal solution. If electrostatic stabilization by ionic species adsorbed on the surface of Pt clusters was the main mechanism assisting the colloidal dispersion of Pt as discussed previously, then the addition of IPA could influence the surface charge of the Pt clusters by displacing some of these ionic species, thereby inducing the aggregation of Pt. This suggestion agrees well with literature reports indicating that the presence of various organic molecules can affect the electrostatic repulsion between Pt clusters by modifying the electric double layer [30]. But the observed aggregation of Pt clusters in the presence of IPA did not lead to any precipitation, suggesting that any modification of the electric double layer was not strong enough to completely eliminate the electrostatic repulsion between the larger Pt aggregates formed. Conversely, taking into account the large excess of IPA in the solution (i.e., IPA/Pt = 1000/1 molar ratio) and its tendency to adsorb strongly on Pt particles [31], we can suggest that IPA also acted as a stabilizing agent, preventing precipitation of Pt. Here its role was somewhat similar to that of PVP or PVA-type compounds. This suggestion concurs with previous reports indicating that Ti and Ru nanoparticles can be stabilized simply by solvent molecules, such as tetrahydrofuran or thioethers [1]; however, the mechanism of such stabilization remains unclear.

When a colloidal suspension containing Pt_6 clusters stabilized by PVA was brought in contact with IPA (0.2 M), the UV–vis spectra revealed a pattern of behavior similar to that observed for the unprotected colloidal Pt suspension. These results suggest that the PVA-protected Pt_6 clusters also underwent some structural changes. Some differences also were observed, however; for example, the absorption band at 215 nm observed in the UV–vis spectrum of the freshly prepared PVA-protected colloidal Pt suspension gradually declined in intensity after the addition of IPA during the first 50 min, and the spectrum remained unchanged thereafter

Table 4
Structural parameters characterizing the Pt species formed in aqueous solutions during 2-propanol (0.2 M) oxidation over an unprotected colloidal Pt suspension

Experiment	Sample	Shell	N	R (Å)	$\Delta\sigma^2$ (Å^2)	ΔE_0 (eV)	ε_v^2	k^1-variances (%)	
								Abs	Im
S3	H_2PtCl_6/H_2O treated with $NaBH_4$ at 25 °C	Pt–Pt	3.1	2.72	0.00325	−6.9	3.0	2.4	3.9
		Pt–O_1	1.9	2.02	0.01000	6.9			
		Pt–O_2	7.3	2.84	0.01000	−10.0			
S3-1	(S3) + IPA	Pt–Pt	7.4	2.74	0.00502	−5.8	1.5	1.5	3.0
		Pt–O_1	0.2	2.02	−0.00992	−3.7			
		Pt–O_2	1.1	2.66	−0.00369	−1.9			
		Pt–O_3	1.1	3.17	−0.00244	−11.8			
S3-2	(S3-1) + O_2 30 min	Pt–Pt	7.7	2.74	0.00466	−8.7	1.7	1.5	2.3
		Pt–O_1	0.6	2.02	0.00500	2.6			
		Pt–O_2	2.4	2.67	0.01000	1.6			
		Pt–O_3	0.8	3.15	−0.00741	−10.1			
S3-3	(S3-1) + O_2 1 h	Pt–Pt	8.9	2.75	0.00568	−6.4	3.5	1.2	1.7
		Pt–O_1	1.2	2.02	0.00477	4.6			
		Pt–O_2	2.4	2.67	0.01000	1.6			
		Pt–O_3	0.8	3.15	−0.00741	−10.1			
S3-4	(S3-1) + O_2 2 h	Pt–Pt	8.7	2.75	0.00520	−5.4	2.1	1.0	1.1
		Pt–O_1	0.9	2.02	0.01000	−3.6			
		Pt–O_2	0.2	2.37	−0.01000	−10.0			
		Pt–O_3	0.3	3.22	−0.00613	−10.1			
S3-5	(S3-1) + O_2 4 h	Pt–Pt	8.8	2.75	0.00543	−5.4	2.8	1.8	1.7
		Pt–O_1	2.1	2.02	0.00500	2.5			
		Pt–O_2	0.1	2.41	−0.01000	10.0			
		Pt–O_3	2.0	3.37	−0.00322	14.4			

Note. Notation as in Table 2.

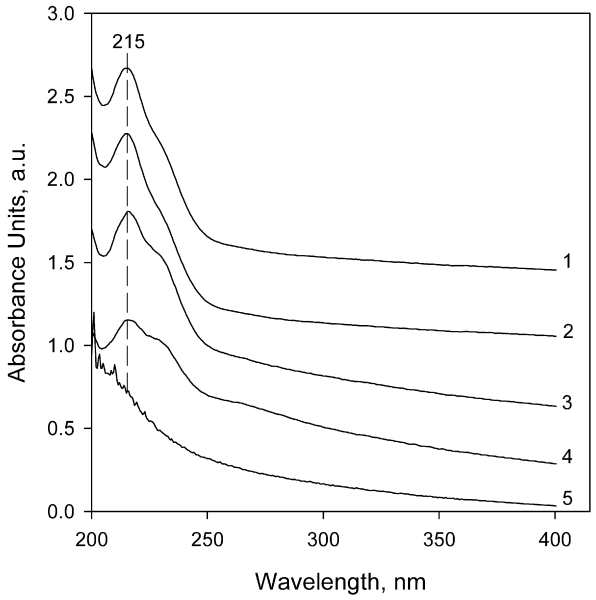

Fig. 7. UV–vis absorption spectra of a PVA-protected colloidal Pt suspension collected at: (1) 0, (2) 10, (3) 20, (4) 30, and (5) 50 min after the addition of IPA.

(Fig. 7). By analogy with the data obtained with the unprotected Pt colloids, these results clearly indicate that in the presence of IPA, aggregation of the Pt_6 clusters occurred in the PVA-protected solution. However, in contrast to what was observed with the unprotected colloidal Pt solution, the aggregation process proceeded at a substantially lower rate, suggesting that the final dispersion of Pt and the degree of aggregation differ substantially from those observed with the unprotected Pt species. In fact, the EXAFS data characterizing the PVA-protected Pt suspension after the interaction with IPA for 50 min indicate the presence of Pt–Pt contributions with an average coordination number of approximately 4.9 at a bond distance of 2.72 Å (Table 5), which is consistent with the formation of colloidal Pt particles with an average diameter of approximately 0.9 nm [29]. The relatively small aggregation of Pt observed in this case can be attributed to the presence of PVA in the solution acting as a steric stabilizing agent and hindering the coagulation of the Pt_6 clusters in the presence of IPA. Therefore, it appears that Pt colloids protected from aggregation by macromolecules, such as PVA, are less likely than unprotected Pt colloids to be affected by the presence of reactants.

3.4. Catalytic oxidation of 2-propanol

The selective catalytic oxidation of alcohols over noble metals has been the focus of numerous investigations due to the importance of this process for the synthesis of fine chemicals [32]. The mechanism of this reaction remains under discussion in the literature despite extensive efforts in this field. It has been suggested that the reaction proceeds via a dehydrogenation phase during which 2-propanol adsorbs on the metal surface and is dehydrogenated in two subsequent steps yielding acetone and hydrogen, which remain on the metal surface [31]. In this mechanism, oxygen plays the role of a scavenger, participating in the oxidation of the adsorbed hydrogen to form water and thus regenerating the metal sites [31]. Another suggested reaction route involves the direct reaction between surface oxygen species and alkoxides formed by dissociative adsorption of alcohols on the metal surface via the abstraction of the hydroxyl hydrogen [31]. The uncertainties regarding the mechanism of this reaction are related primarily to difficulties in identifying reaction intermediates by *in situ* spectroscopic techniques on the catalyst surface and the metal-liquid interface. Nevertheless, some literature reports indicate an increased turnover frequency with decreasing Pt dispersion on various supports (e.g., SiO_2, γ-Al_2O_3, and carbon), suggesting that the reaction is structure-sensitive and favored over larger Pt particles [31].

We used the selective oxidation of IPA to acetone as a test reaction to evaluate the catalytic activity of Pt colloidal suspensions. When both the unprotected and PVA-protected suspensions were brought in contact with 2-propanol and O_2 was introduced to the

Table 5
Structural parameters characterizing the Pt species formed in aqueous solutions during 2-propanol (0.2 M) oxidation over a PVA-protected colloidal Pt suspension

Experiment	Sample	Shell	N	R (Å)	$\Delta\sigma^2$ (Å^2)	ΔE_0 (eV)	ε_ν^2	k^1-variances (%)	
								Abs	Im
S4	H_2PtCl_6/H_2O treated with $NaBH_4$ at 25 °C in presence of PVA	Pt–Pt	4.1	2.73	0.00581	−6.1	4.6	1.2	2.0
		Pt–O_1	0.4	2.01	−0.00160	0.15			
		Pt–O_2	6.0	2.25	0.00659	−8.9			
		Pt–O_3	8.7	2.45	0.00895	7.0			
S4-1	S4 + IPA	Pt–Pt	4.9	2.72	0.00697	−0.2	1.2	1.2	1.9
		Pt–O_1	1.1	2.05	−0.00303	−4.3			
		Pt–O_2	6.4	2.26	0.00409	−10.0			
		Pt–O_3	9.6	2.42	0.00694	6.2			
S4-2	(S4-1) + O_2 1 h	Pt–Pt	8.3	2.73	0.00679	−4.7	1.8	3.0	4.6
		Pt–O_1	0.5	2.02	−0.00121	3.3			
		Pt–O_2	0.4	2.37	0.00694	10.0			
		Pt–O_3	0.4	3.16	−0.00653	−7.6			
S4-3	(S4-1) + O_2 2 h	Pt–Pt	8.5	2.73	0.00682	−3.7	2.8	2.4	4.8
		Pt–O_1	0.9	2.02	0.00574	2.3			
		Pt–O_2	0.7	2.50	0.01000	−0.6			
		Pt–O_3	0.4	3.12	−0.00648	−4.1			
S4-4	(S4-1) + O_2 3 h	Pt–Pt	8.6	2.73	0.00705	3.6	1.6	3.4	4.0
		Pt–O_1	0.6	2.02	−0.00028	2.3			
		Pt–O_2	0.7	2.50	0.01000	0.5			
		Pt–O_3	0.6	3.12	−0.00654	−4.1			
S4-5	(S4-1) + O_2 4 h	Pt–Pt	8.8	2.73	0.00699	−3.6	1.0	2.8	4.6
		Pt–O_1	0.8	2.02	0.00056	4.5			
		Pt–O_2	0.8	2.50	0.01000	0.5			
		Pt–O_3	0.6	3.19	−0.00243	−9.5			

Note. Notation as in Table 2.

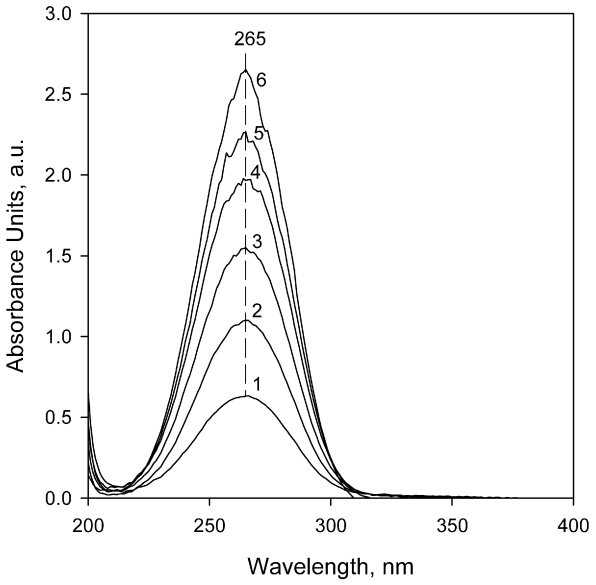

Fig. 8. UV–vis absorption spectra collected during the oxidation of IPA to acetone over an unprotected Pt colloidal suspension at: (1) 30, (2) 60, (3) 90, (4) 120, (5) 180, and (6) 240 min after the onset of the reaction.

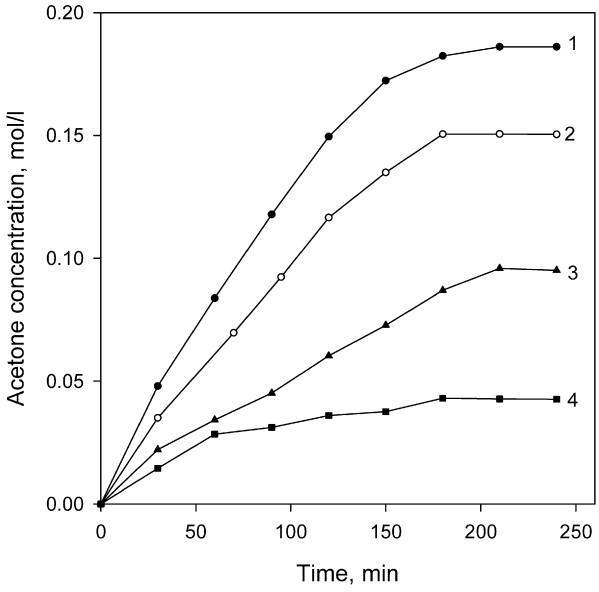

Fig. 9. Acetone concentration profiles as functions of reaction time collected during the oxidation of IPA over an unprotected colloidal Pt suspension at different initial concentrations of IPA: (1) 0.2, (2) 0.15, (3) 0.1, and (4) 0.05 M.

solution, acetone did not appear until after approximately 30 and 50 min, respectively. However, during this induction period, the 215-nm band in the UV–vis spectra decreased in intensity, accompanied by increased absorption intensity at higher wavelengths. These changes are similar to those observed for both colloids during aging in the presence of IPA, suggesting the formation of larger Pt aggregates during the induction period in both cases. Independent experiments performed with both colloids have demonstrated that the addition of O_2 into solutions that had been already aged in the presence of IPA leads to the immediate formation of acetone. These results suggest that the selective oxidation of IPA to acetone does not proceed over the small Pt_4 and Pt_6 clusters present in the original colloidal solutions, but instead, larger Pt aggregates are required, which are formed during the aging in the presence of IPA. These results are in agreement with previously published theoretical calculations [33] indicating that at least 3 metal atoms are required to accommodate the alkoxide molecule, presumably formed as a result of the dissociative adsorption of IPA on Pt; therefore, the Pt_4 and Pt_6 clusters initially present in the unprotected and PVA-protected colloidal Pt suspensions, respectively, would have an insufficient number of free surface sites to simultaneously accommodate all surface species involved in this reaction scheme (i.e., alkoxide, hydrogen, and oxygen). Consequently, the induction period observed during catalytic experiments, which coincides with growth of Pt particles in the solution after the addition of IPA, reconfirms the structure-sensitive nature of the reaction and indicates that a critical metal particle size (approximately 1 nm) is required for the selective oxidation of 2-propanol to proceed at any significant extent.

UV–vis absorption spectra collected at different times during the oxidation of IPA to acetone over an unprotected colloidal Pt suspension are shown in Fig. 8. The absorption arising from the Pt colloid has been subtracted from these spectra by referencing them to an IPA-containing colloidal Pt solution that was not in contact with O_2. The plots illustrating the changes in the concentration of acetone in the solution as a function of the reaction time are shown in Fig. 9 for different initial IPA concentrations. The induction period has been removed from these plots, so that the zero point of the reaction time corresponds to the end of the induction period. These results demonstrate that nearly complete conversion of IPA to acetone was achieved after 4 h for all concentrations examined. The slopes of these curves can be used to obtain the initial reactions rates given in Table 6. These rates suggest that the IPA oxidation closely followed first-order kinetics with respect to the IPA concentration. The reaction rates were found to be independent of the stirring conditions, indicating the absence of mass transfer limitations in our system.

Table 6
Rates for the oxidation of 2-propanol catalyzed by colloidal Pt suspensions

Sample	Initial concentration of IPA (mol/L)	Reaction rate[a] (mmol acetone/(mmol Pt min))
Unprotected colloidal Pt suspension	0.20	6.5
Unprotected colloidal Pt suspension	0.15	4.5
Unprotected colloidal Pt suspension	0.10	2.9
Unprotected colloidal Pt suspension	0.05	1.9
PVA-protected colloidal Pt suspension (Pt/PVA = 1/1)	0.20	4.8
PVA-protected colloidal Pt suspension (Pt/PVA = 1/2)	0.20	0.8

[a] Rates obtained at 14 °C, atmospheric pressure, and Pt concentration of $2.6 \cdot 10^{-4}$ M.

Similar experiments were also performed with PVA-protected colloidal Pt suspensions. Fig. 10 compares the catalytic performance of the unprotected and PVA-protected suspensions under identical experimental conditions. The PVA-protected suspensions exhibited lower acetone formation rates (Table 6), which were further influenced significantly by the Pt/PVA ratio used. At a Pt/PVA ratio of approximately 1/1 by weight, a decrease of approximately 25% was observed in the reaction rate with respect to the unprotected suspension. When the amount of PVA in solution was doubled (Pt/PVA = 1/2), the reaction rate decreased by sixfold. Not only the reaction rates, but also the final yield of acetone, decreased accordingly, suggesting an overall poisoning effect by PVA, which can be attributed to a “shielding” of the active Pt sites by adsorbed PVA and/or acetone species.

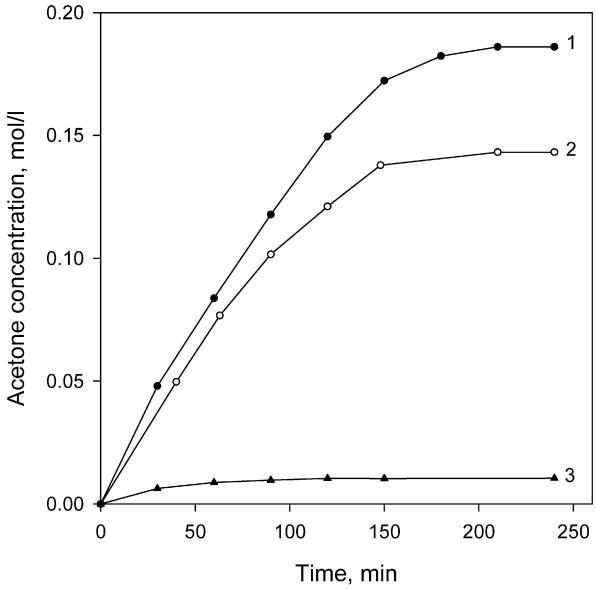

Fig. 10. Acetone concentration profiles as functions of reaction time collected during the oxidation of IPA (0.20 M) over: (1) an unprotected colloidal Pt suspension, and PVA-protected colloidal Pt suspensions with Pt/PVA weight ratios of (2) 1/1 and (3) 1/2.

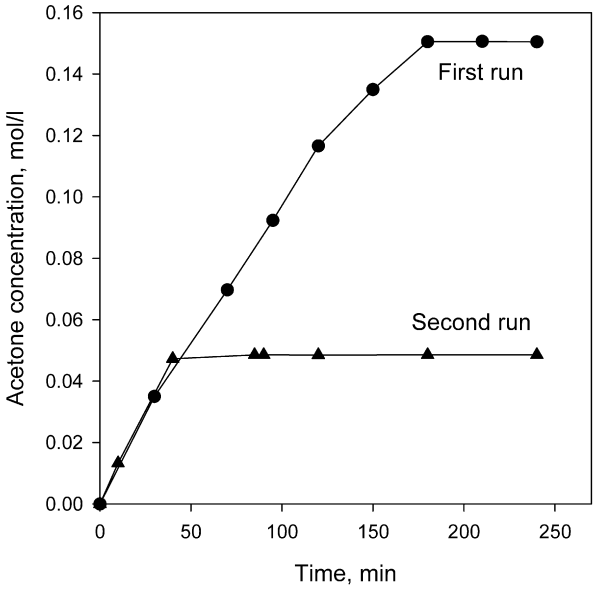

Fig. 11. Acetone concentration profiles as functions of reaction time collected during the oxidation of IPA (0.15 M) over an unprotected colloidal Pt suspension during two subsequent runs.

Literature reports indicate that when SiO_2-, γ-Al_2O_3-, and carbon-supported Pt catalysts were used for the oxidation of IPA to acetone in aqueous solutions, a substantial deactivation of these catalysts was observed. This behavior was attributed primarily to the irreversible oxidation of surface Pt atoms by the oxygen present, leading to the formation of platinum oxide species that are inactive for this reaction [31]. The XANES data reported in Table 3 for unprotected and PVA-protected colloidal Pt suspensions indicate that the white line areas characterizing these samples under reaction conditions were almost the same as those characterizing the same samples before they were exposed to the reactants. These results suggest that oxidation of Pt apparently did not occur under our reaction conditions.

Nevertheless, we performed the IPA oxidation twice over the same unprotected colloidal Pt suspension; the results obtained for these two consecutive runs are shown in Fig. 11. When the first run was completed, 0.15 M of IPA was added to the reaction mixture and the experiment was continued. Fig. 11 shows that acetone was formed at nearly the same rate during the first 40 min of the second run, but that its formation ceased abruptly thereafter. This suggests that although no catalyst deactivation appeared to be occurring initially, the reaction was poisoned by acetone once its overall concentration in the solution exceeded 0.2 M. This finding agrees with several previous reports indicating that acetone can significantly slow the dehydrogenation of IPA over Ni surfaces [31]. Consequently, the oxidation of IPA over Pt also would be expected to be inhibited by acetone, due to the competitive adsorption of acetone and IPA on the same metal sites [31].

To determine whether the oxidation of IPA can induce any changes in the structure of the colloidal Pt particles, we characterized the local environment of Pt under reaction conditions by *in situ* EXAFS, using an initial IPA concentration of 0.2 M. The results of the EXAFS data analysis are summarized in Tables 4 and 5. When the reaction was performed with an unprotected colloidal Pt suspension, the average first-shell Pt–Pt coordination number increased progressively from 7.4 to 8.9 during the first 60 min of the reaction and remained nearly unchanged thereafter (Table 4). When similar experiments were performed with the PVA-protected colloidal Pt suspension with a Pt/PVA weight ratio of 1, the average first-shell Pt–Pt coordination number once again increased under reaction conditions from 4.9 to 8.3 during the first 60 min (Table 5). In both cases, the observed increase in the Pt–Pt first-shell coordination number indicates that some sintering of Pt occurred in these solutions under the influence of reactants, intermediates, and/or products. Such sintering occurred only during the early stages of the reaction. The average particle size of Pt eventually obtained, and subsequently maintained in the stabilized solution under reaction conditions, was calculated [29] as 2.3 nm for the unprotected suspensions and 1.8 nm for the PVA-protected suspensions. Even though these results suggest that a slightly better dispersion of Pt was maintained in the PVA-protected suspension, given experimental uncertainties it could be argued that both types of suspensions exhibited roughly the same degree of sintering under reaction conditions.

In addition to the Pt–Pt contributions, Pt–O contributions at an average distance of 2.02–2.05 Å were also observed in the first coordination shell of Pt under reaction conditions for both colloidal suspensions (Tables 4 and 5). These contributions characterize the interactions of Pt particles with aquo ligands, acetone, and/or oxygen adsorbed on the Pt surface. It is interesting to note that when the reaction was performed with the unprotected colloidal Pt suspension, the average Pt–O coordination number increased gradually with reaction time, reaching a value of approximately 2.1 at the completion of the reaction (Table 4). In contrast, when the oxidation of IPA was performed with a PVA-protected suspension, the average Pt–O coordination number remained nearly the same regardless of the IPA conversion.

Since the various Pt–O contributions arising from different oxygen-containing compounds present in the solution cannot be distinguished by EXAFS, we can only speculate as to why such differences were observed between the two suspensions investigated. In the case of the unprotected suspension, both the addition of IPA and its subsequent reaction with O_2 led to a relatively rapid nucleation of Pt_4 clusters to nanoparticles with average dimensions of 1.4 and 2.3 nm, respectively. More importantly, no precipitation of Pt was observed during this time, and the solution (although containing such relatively large Pt particles) was stable for several months in the presence of the acetone formed. However, when acetone was removed from the solution by purging with nitrogen, the precipitation of black Pt aggregates was observed. Consequently, the high stability of Pt nanoparticles in the unprotected

suspension can be attributed to acetone and its role as a steric-stabilizing agent. Moreover, because the concentration of acetone in the solution (and thus adsorbed on the Pt surface through the carbonyl functional group) increased with reaction time, an increase of the Pt–O contributions would be expected, consistent with our experimental observations (Table 4). In contrast, in the PVA-protected suspensions, the PVA macromolecules were already strongly bonded to the Pt surface, and thus some fraction of the Pt surface atoms was not available for reaction [1,4]. This property is reflected in the lower overall activity of the PVA-protected colloidal Pt suspension for the IPA oxidation (Table 6). In this case, estimating the fraction of Pt surface atoms blocked by PVA is not possible, but we can assume that the fraction of available sites was too small to allow detection of any significant changes in the Pt–O contribution under reaction conditions by EXAFS.

Finally, the values of the white line area characterizing both suspensions under reaction conditions were nearly the same as those determined for the fresh suspensions before their exposure to the reactants. Therefore, in contrast to what has been suggested previously for supported Pt catalysts [31], the analysis of the XANES region of the spectra indicates that Pt remained in the reduced state in both the unprotected and PVA-protected suspensions under reaction conditions and was not oxidized by the molecular oxygen present in the solution.

4. Conclusion

Unprotected and PVA-protected colloidal Pt suspensions containing nearly uniform Pt_4 and Pt_6 clusters, respectively, were prepared by treatment of an aqueous solution of H_2PtCl_6 with $NaBH_4$. Both suspensions were found to be stable for several months. The interaction of 2-propanol with these colloidal Pt suspensions at room temperature led to the aggregation of the Pt clusters into larger nanoparticles; however, no signs of Pt precipitation were observed in either case, indicating that 2-propanol acted as a stabilizing agent under these conditions, especially in the unprotected suspension. Both suspensions were active for the selective oxidation of 2-propanol to acetone, following first-order kinetics in 2-propanol. The unprotected suspension exhibited greater catalytic activity than the PVA-protected one, indicating that the presence of PVA reduced the catalytic efficiency of the Pt nanoparticles for this reaction.

Acknowledgments

This work was supported by the U.S. Department of Energy, Office of Basic Energy Sciences (DE-FG02-05ER14980). A part of this research was carried out at the Stanford Synchrotron Radiation Laboratory (SSRL), a national user facility operated by Stanford University on behalf of the U.S. Department of Energy, Office of Basic Energy Sciences. The authors thank the beam line staff at SSRL for their assistance. The EXAFS data were analyzed using the XDAP software developed by Vaarkamp et al. [5].

References

[1] A. Roucoux, J. Schulz, H. Patin, Chem. Rev. 102 (2002) 3757.
[2] C. Burda, X. Chen, R. Narayanan, M.A. El-Sayed, Chem. Rev. 105 (2005) 1025.
[3] B.L. Cushing, V.L. Kolesnichenko, C.J. O'Connor, Chem. Rev. 104 (2005) 3893.
[4] R.M. Crooks, M. Zhao, L. Sun, V. Chechik, L.K. Yeung, Acc. Chem. Res. 34 (2001) 181.
[5] M. Vaarkamp, J.C. Linders, D.C. Koningsberger, Physica B 208–209 (1995) 159.
[6] D.C. Koningsberger, in: C.A. Melendres, A. Tadjeddine (Eds.), Synchrotron Techniques in Interfacial Electrochemistry, Kluwer, Dordrecht, 1994, p. 181.
[7] E.A. Stern, Phys. Rev. B 48 (1993) 9825.
[8] E.O. Brigham, The Fast Fourier Transform, Prentice–Hall, Englewood Cliffs, NJ, 1974.
[9] P.S. Kirlin, F.B.M. van Zon, D.C. Koningsberger, B.C. Gates, J. Phys. Chem. 94 (1990) 8439.
[10] J.B.A.D. van Zon, D.C. Koningsberger, H.F.J. van't Blik, D.E. Sayers, J. Chem. Phys. 82 (1985) 5742.
[11] M. Vaarkamp, Ph.D. thesis, Eindhoven University, The Netherlands, 1993.
[12] F.W. Lytle, D.E. Sayers, E.A. Stern, Physica B 158 (1988) 701.
[13] D.C. Koningsberger, B.L. Mojet, G.E. van Dorssen, D.E. Ramaker, Top. Catal. 10 (2000) 143.
[14] J.H. Sinfelt, in: Y. Iwasawa (Ed.), X-Ray Absorption Fine Structure for Catalysts and Surfaces, World Scientific Publishing, Singapore, 1996.
[15] J.H. Sinfelt, G.D. Meitzner, Acc. Chem. Res. 26 (1993) 1.
[16] W.A. Spieker, J. Liu, J. Kropf, J.T. Miller, J.R. Regalbuto, Appl. Catal. A 232 (2002) 219.
[17] J.P. Boitiaux, J.M. Deves, B. Dillion, C.R. Macilly, in: G.J. Antos, A.M. Aitani, J.M. Parera (Eds.), Catalytic Naphtha Reforming, Science and Technology, Marcel Dekker, New York, 1995, p. 79.
[18] L. Gmelin, R.J. Meyer, in: Gmelins Handbuch der Anorganischen Chemie, Platin, vol. Teil C Lieferung 1, 8 Auflage, Verlag Chemie, Weinheim, 1939.
[19] O.S. Alexeev, A. Siani, G. Lafaye, C.T. Williams, H.J. Ploehn, M.D. Amiridis, J. Phys. Chem. B 110 (2006) 24903.
[20] A. Siani, O.S. Alexeev, C.T. Williams, H.J. Ploehn, M.D. Amiridis, X-Ray Absorption Fine Structure, AIP Conference Proceedings 882 (2007) 737.
[21] R. Ayala, E.S. Marcos, S. Diaz-Moreno, V.A. Sole, A. Muñoz-Páez, J. Phys. Chem. B 105 (2001) 7588.
[22] B. Shelimov, J. Lambert, M. Che, B. Didillon, J. Catal. 185 (1999) 462.
[23] A. Henglein, B.G. Ershov, M. Marlow, J. Phys. Chem. 99 (1995) 14129.
[24] D.N. Furlong, A. Launikonis, W.H.F. Sasse, J.V. Sanders, J. Chem. Soc. Faraday Trans. 1 80 (1984) 571.
[25] D.N. Furlong, W.H.F. Sasse, Aust. J. Chem. 36 (1983) 2163.
[26] L.C. Ciacchi, W. Pompe, A. De Vita, J. Phys. Chem. B 107 (2003) 1755.
[27] A. Henglein, M. Giersig, J. Phys. Chem. B 104 (2000) 6767.
[28] L.C. Ciacchi, W. Pompe, A. De Vita, J. Am. Chem. Soc. 123 (2001) 7371.
[29] B.J. Kip, F.B.M. Duivenvoorden, D.C. Koningsberger, R. Prins, J. Catal. 105 (1987) 26.
[30] J. Newman, K.E. Thomas-Ayela, Electrochemical Systems, Wiley, Chichester, 2004.
[31] J.W. Nicoletti, G.M. Whitesides, J. Phys. Chem. 93 (1989) 759.
[32] T. Mallat, A. Baiker, Chem. Rev. 104 (2004) 3037.
[33] T. Bürgi, M. Bieri, J. Phys. Chem. B 108 (2004) 13364.